Chemical Physics 530 (2020) 110645

Contents lists available at ScienceDirect

Chemical Physics

journal homepage: www.elsevier.com/locate/chemphys

New stable phases of glycine crystals

Doris Guerra[a], Luis A. Gómez[b], Albeiro Restrepo[a,*], Jorge David[c,*]

[a] Instituto de Química, Universidad de Antioquia UdeA, Calle 70 No. 52-21, Medellín, Colombia
[b] Escuela de Ciencias, Departamento de Ciencias Biológicas, Universidad EAFIT, Medellín, Colombia
[c] Escuela de Ciencias, Departamento de Ciencias Físicas, Universidad EAFIT, Medellín, Colombia

A B S T R A C T

A Density Functional Theory (DFT) study of the electronic, energetic, dynamical, and mechanical properties of new glycine molecular crystals is presented here. Our search of the potential energy surface (PES) reproduces the previously reported structures for α-, β-, and γ-glycine with $P2_{1/n}$, $P2_1$, $P3_1$ symmetries, respectively. In addition, we report three new orthorhombic (o), tetragonal (t), and monoclinic (m) crystals with $P2_12_12_1$, $P4_3$, and $P2_1$ symmetries. The crystals have wide band gaps, classifying them in the range of insulators. All three new phases have low mechanical hardness (< 3.2 GPa), characterizing them as soft crystals. Topological and local energetic properties of the electronic densities for the new crystalline phases of glycine have been calculated using the tools provided by the quantum theory of atoms in molecules (QTAIM) under periodic conditions. Typical NH···O, OH···O as well as secondary CH···O hydrogen bonds (HBs), act as the stabilizing factors resulting in large cohesive energies for the new phases of glycine crystals. Without exception, all types of HBs, for all new phases, perfectly fit the attractive region of a Lennard-Jones potential.

1. Introduction

For many years, determining the properties of amino acid crystals has been a hot research topic. These properties are very important, among others, in industrial applications, in the development of biosensors and optoelectronic devices [1]. In this context, it appears that alanine, leucine, isoleucine, valine, and glycine crystals are all insulators [2–4]. In particular, glycine is a very promising material in optoelectronic applications [5,6], and its ferro-optical properties lead to applications in medicine and biology [7]. Recently, Hu and coworkers [8] studied the bioferroelectric properties of glycine crystals, helping in the rationalization of electric dipole organization in biomaterials.

Glycine is the structurally simplest amino acid: it does not contain substituents at the α-carbon and as a consequence is not a chiral molecule. There are three known stable phases of glycine crystals at room conditions, labeled α, β, γ-glycine [9,10]. Under high humidity conditions α and β-glycine are transformed into γ-glycine [11]. Metastable δ, ξ-glycine phases, only observable at high pressures, have also been reported [12].

Chisholm et al. [4] investigated crystalline structures of glycine and their thermodynamic stabilities using *ab initio* techniques, however, there are no reports of dynamic and mechanical stabilities of glycine crystals. Maron and coworkers gave a complete description of the structures and stabilities of the crystalline polymorphs of α, β and γ-glycine using density functional theory [13]. New glycine polymorphs are of great interest, since modulation of their properties may lead to new developments [14–16]. In this work, we present new glycine crystal structures that meet energetic, dynamic, and mechanical stability criteria.

2. Computational details

A stochastic search for molecular crystals of glycine was carried out using evolutionary algorithms as implemented in the USPEX code [17–19]. At this point, it is quite important to explicitly state that the initial structures for the stochastic search where constructed using only the zwitterion form of glycine. Notice that although the zwitterion form is the most common one found in glycine crystals, any configuration is contingent to experimental conditions [20]. The structural and electronic properties of all calculated crystals were analyzed using Density Functional Theory (DFT) [21–23]. The CRYSTAL-14 [24,25] program was used to optimize crystal geometries and lattice parameters. Harmonic vibrational frequencies and mechanical properties of all the crystalline structures generated by USPEX were also computed. Besides the already known molecular crystals of α-glycine with $P2_{1/n}$ symmetry, β-glycine with $P2_1$ symmetry, and γ-glycine with $P3_1$ symmetry, our calculations yielded new stable phases, surprisingly, one of them containing pristine glycine molecules, not in the zwitterion form. Our strategy comprises all electron DFT calculations using linear combination of atomic orbitals (LCAO) in conjunction with the hybrid B3LYP functional [26–28] as implemented in CRYSTAL-14. Gaussian basis sets with triple-zeta valence and polarization [29] were used for carbon,

* Corresponding author.
E-mail addresses: albeiro.restrepo@udea.edu.co (A. Restrepo), jdavidca@eafit.edu.co (J. David).

https://doi.org/10.1016/j.chemphys.2019.110645
Received 1 October 2019; Received in revised form 27 November 2019; Accepted 27 November 2019
Available online 30 November 2019
0301-0104/

Table 1
Space group, lattice parameters, and %error in the volume of the unit cell with respect to the experimentally known [31] glycine crystals. The very recent dispersion corrected GGA results [32], and our own calculations are shown. n is the number of monomers per unit cell. All calculations in this work using B3LYP in conjunction with a triple-zeta valence plus polarization basis set.

System	n	Space Group	Method	a/Å	b/Å	c/Å	α, β, γ	%error(V)
γ-glycine	3	$P3_1(144)$	Experimental	7.0383(7)	—	5.4813(8)	—	
			GGA + TS_{1100}	7.08	—	5.49	—	1.4
			This work	7.20	—	5.52	—	5.8
α-glycine	4	$P2_{1/c}(14)$	Experimental	5.1047(3)	11.9720(14)	5.4631(3)	111.740(5)	
			GGA + TS_{1100}	5.12	11.97	5.46	111.12	0.2
			This work	5.23	13.89	5.48	110.03	20.17
β-glycine	2	$P2_1(4)$	Experimental	5.0932(16)	6.272(3)	5.3852(18)	113.19(3)	
			GGA + TS_{1100}	5.09	6.32	5.39	112.69	1.0
			This work	5.17	6.49	5.40	111.03	6.9

Table 2
Optimized geometric parameters for α, β, γ glycine and the new o, t, and m phases of glycine crystals. See Fig. 2 for atom labels.

	α-Glycine		β-Glycine		γ-Glycine		o	t	m
Bond Lengths	This work	Exp [40]	This work	Exp [10]	this work	Exp [41]			
O1-C3	1.26	1.256(1)	1.26	1.247(4)	1.27	1.258(1)	1.43	1.25	1.24
O2-C3	1.26	1.258(1)	1.27	1.254(4)	1.26	1.247(2)	1.33	1.27	1.29
C3-C4	1.53	1.524(1)	1.53	1.530(3)	1.53	1.531(1)	1.55	1.53	1.52
C4-N5	1.49	1.479(1)	1.49	1.474(4)	1.49	1.473(1)	1.50	1.50	1.49
N5-H6	1.03	1.034(1)	1.04	0.90	1.03	1.034(2)	1.06	1.04	1.04
N5-H7	1.06	1.056(1)	1.05	0.88	1.05	1.053(1)		1.04	1.03
N5-H8	1.04	1.041(1)	1.03	0.90	1.04	1.040(2)	1.02	1.05	1.04
C4-H9	1.09	1.094(1)	1.09	0.95	1.09	1.086(3)	1.09	1.08	1.08
C4-H10	1.09	1.095(1)	1.09	0.97	1.09	1.093(3)	1.09	1.09	1.09
O2-H7							0.99		
Bond Angle									
O1-C3-O2	125.50	125.46	125.68	125.9(3)	125.54	125.8(1)	115.68	125.79	125.80
O1-C3-C4	117.63	117.36	117.47	117.1(3)	118.07	117.7(1)	112.00	117.34	119.31
O2-C3-C4	116.86	117.17	116.80	116.9(2)	116.35	116.5(1)	110.55	116.86	114.89
C3-C4-N5	111.38	111.50	112.71	111.6 (2)	111.93	111.5(1)	113.09	111.42	112.18
H7-O2-C3							111.63		
C4-N5-C3							121.00		
Torsion Angle									
O2-C3-C4-N5	143.40		152.70		162.50	167.1(1)	162.80	116.20	167.30
O1-C3-C4-N5	38.10	18.60	29.50	24.80	19.60	15.4(1)	32.20	62.60	13.50
H7-O2-C3-C4							46.50		
H7-O2-C3-N5							156.50		

nitrogen, oxygen and hydrogen. Justification for this choice of model chemistry is provided in Table 1 and in Table 2, were the experimental parameters and the very accurate dispersion corrected GGA calculations of Rodríguez and coworkers [32] for the known glycine crystals are meticulously reproduced with the single exception of the b parameter for the α crystal. Notice that this error is consistent with the GGA calculations of Rodríguez with no correction for dispersion. This single error appears to have no consequences in our further analysis since all other lattice parameters, bond distances, and cohesive energies for the three known crystals are correctly reproduced. For the calculations reported in Table 1, Brillouin zone integration was performed on a Monkhorst-Pack [30] $12 \times 12 \times 12$ **k**-mesh.

It is now well established that B3LYP is good enough to reproduce crystal geometries in the systems studied here, unfortunately, cohesive energies mandate the inclusion of dispersion. Indeed, a total of 14 molecular crystals bonded via hydrogen bonds were studied by Civalleri and coworkers [33], who explicitly wrote "*The dispersion correction is crucial to arrive at a reasonable agreement with experiment. In fact, the pure B3LYP method gives results that are rather poor. The cohesive energies are generally underestimated in many cases, mainly for dispersion bonded molecular crystals (e.g. propane, C_6H_6, naphthalene, …) they become repulsive. ⋯ The inclusion of the dispersion term in the original parameterization proposed by Grimme leads to a dramatic improvement and a good agreement with experimental data.*" Accordingly, we report here cohesive energies corrected by Grimme dispersion.

3. Results and discussion

3.1. Geometries

Geometrical parameters for glycine molecules in the new crystalline phases are listed in Table 2. Lattice parameters and spatial groups are listed in Table 3.

The molecular packing of the new crystalline structures of glycine are shown in Fig. 1. The calculated new phases of glycine exhibit different arrays of molecular packing and a variety of intermolecular interactions. The monoclinic (m) and tetragonal (t) phases, as well as the

Table 3
Space group and lattice parameters of the new crystals of glycine. n is the number of monomers per unit cell.

System	n	Space Group	a/Å	b/Å	c/Å	α, β, γ
m-glycine	4	$P2_1(4)$	4.79	7.38	10.08	103.64
t-glycine	4	$P4_3(78)$	6.39	—	8.50	—
o-glycine	4	$P2_12_12_1(19)$	5.80	5.22	10.19	—

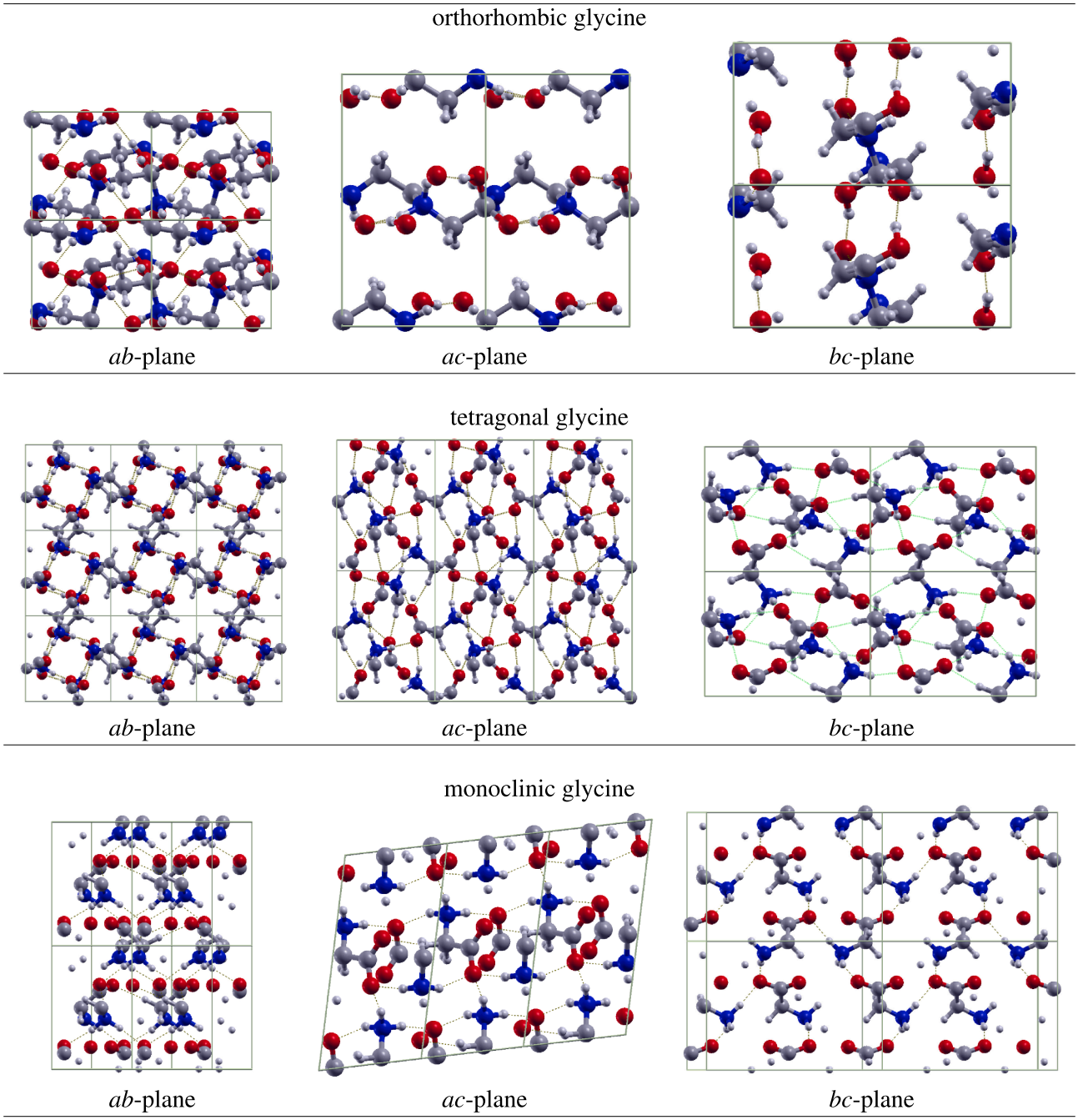

Fig. 1. Molecular packing in the new o-, t- and m-glycine crystal structures. Color code: Carbon: grey, Hydrogen: small white spheres, Nitrogen: blue, Oxygen: red. Hydrogen bonds are represented by dashed lines.

well known α phase, retain glycine monomers in the zwitterion form (See Fig. 2). In contrast, in the orthorhombic (*o*) phase, the zwitterion form is lost in favor of long chains of glycine molecules linked through a highly covalent interaction (see below) between the carbonyl carbon on one glycine to the amino nitrogen of the neatest neighbor affording a C3···N5 distance of 1.57 Å. Because of these interactions, along the entire chain, one of the hydrogen atoms in the quaternary ammonium end of the zwitterion (H7, Fig. 2) is transferred to one of the oxygen atoms of the $-CO_2^-$ group of another neighbor, leading to the formation of the O1-H7 bond (0.99 Å) (see Fig. 2).

In the new orthorhombic phase, the newly formed $H_2N\cdots C{=}O$ group participates in two equivalent, strong hydrogen bonds (O2···H6N5 (1.62 Å) in Fig. 2), where the NH_2 group acts as a proton donor to a C=O group. These hydrogen bonds are responsible for the two dimensional folding of the chains which extends along the *a*-axis (*ac*-plane of *o*-glycine in Fig. 1). A hydrogen bond inter layer between folded chains is formed by the O2···H7O1 interaction (1.72 Å) along the *b* axis, resulting in two-dimensional layers stacked along the *c* axis (*bc*-plane of *o*-glycine in Fig. 1). *o*-glycine crystallizes in the $P2_12_12_1$ space group with 4 formula units per unit cell (see Table 3).

The new tetragonal phase of glycine crystallizes in the $P4_3$ space group with four formula units per unit cell. We describe this *t* phase as a centrosymmetric crystal structure, with the glycine molecules adopting a tetramer rhombus-like geometry localized at the center of the conventional cell, as seen from the *ab* plane (see the middle panel of Fig. 1). The four monomers are held together within the unit cell by the O2···H8N (1.74 Å), O2···H6N (1.81 Å), O1···H7N (1.86 Å), and O1···H9C (2.13 Å) hydrogen bonds (see Fig. 2). This arrangement of the

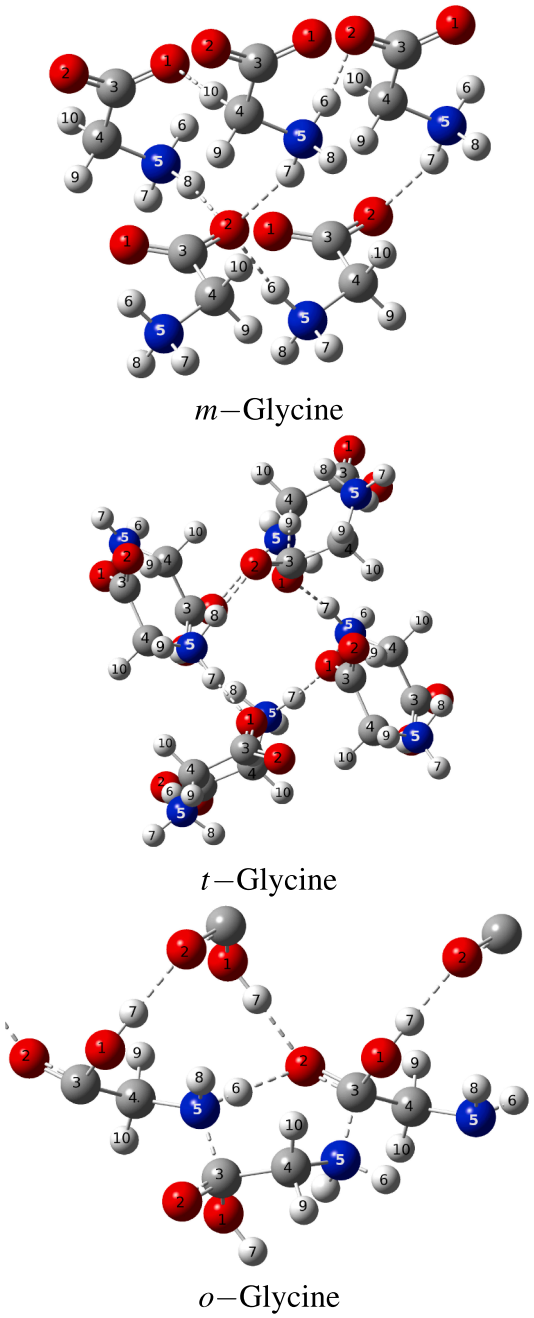

Fig. 2. Atom numbering for the *m*-, *t*- and *o*-glycine. Color code: Carbon: grey, Hydrogen: small white spheres, Nitrogen: blue, Oxygen: red. Hydrogen bonds are represented by dashed lines.

glycine monomers within the unit cell that propagates throughout the crystal results in a strong 3D network of hydrogen bonds.

The new monoclinic phase, shows a very interesting array in which the atoms labeled O2 in Fig. 2 act as acceptors of three hydrogen bonds. As seen from the *bc*-plane (Fig. 1), individual glycine molecules in the zwitterion form adopt the same configuration for the $-CO_2^-$ group, simultaneously alternating configurations of the $-C(NH_3)^+$ groups between adjacent layers. The four monomers per unit cell interact via O2···H8N5 (1.85 Å), O2···H6N5 (1.88 Å), and O2···H7N5 (1.98 Å) hydrogen bonds.

Notice that in all new phases of glycine crystals predicted here, secondary hydrogen bonds of the C–H···O type are stabilizing factors. See for example the *ac*-plane in tetragonal glycine in Fig. 1, and the corresponding data listed in Table 8, which will be analyzed in detail below.

3.2. Cohesion energies

In order to estimate the energetic stability of glycine crystals, cohesive energies per molecule were calculated using

$$E_{\text{cohesion}} = \frac{E_{\text{crystal}}}{n} - E_{\text{molecule}} \quad (1)$$

where E_{crystal} is the crystal energy, n is the number of molecules in the unit cell, and E_{molecule} is the total energy of the equilibrium geometry of the isolated molecule in the gas phase. This is the energy necessary to dissociate the crystal into separated molecules. Zero point energies (ZPE) and empirical D3 Grimme dispersion corrections [34] were used to accurately compute lattice energies as well as molecular gas phase energies. ZPE of the glycine crystals were obtained through the full set of vibrational frequencies computed at the Γ point [35]. Corrected cohesive energies per molecule of the new molecular crystals are −64.12, −146.31, and −167.94 kJ/mol for the orthorhombic, tetragonal, and monoclinic phases, respectively. On the grounds of these cohesion energies, the new crystals of glycine found here appear to be thermodynamically stable. Moreover, using our computational method, we obtained corrected cohesive energies per molecule of −158.31, −172.75, and −175.50 kJ/mol for the experimentally known monoclinic α, β, and trigonal γ phases, respectively. These results are very encouraging because it seems that our approach recovers what is known about glycine crystals [13,36–39,10,42–45], thus, providing strong support to the new stable phases.

4. Dynamic and electronic properties

Lattice dynamics is an important branch of condensed matter physics and is critical for understanding the thermal properties of crystalline solids at finite temperatures [46,47]. As a matter of fact, densities of phonon states are required to evaluate thermal expansion coefficients, heat capacities, entropies and lattice thermal conductivity of crystals, among other thermodynamic properties [48–53]. In order to be able to compute the dynamic vibrational matrix at different high symmetry points of the Brillouin zone, a 2 × 2×2 supercell was employed. Frequencies for vibrational normal modes were calculated within the harmonic approximation by numerical differentiation of the analytical gradient of the potential energy with respect to atomic positions [35]. All phonon frequencies for the new orthorhombic, tetragonal, and monoclinic phases are positive, thus describing dynamically stable crystals.

Calculations of band structures and of density of states afford valuable information to study electronic properties of crystals, specifically, gaps between valence and conduction bands determine the ability of extended crystals to transport and conduct electric charge. According to Tulip and Clark [2], calculated band gaps for crystals of common amino acids are 5.27, 5.07, 5.05, and 4.68 eV for valine, alanine, leucine, and isoleucine, respectively. For serine, Costa and coworkers [54] measured a 5.90 eV band gap. Cândido-Júnior and coworkers [55] reported an experimental band gap for cysteine (orthorhombic) of 4.68 ± 0.02 eV. Similarly, for α-glycine [3] ($P2_12_12_1$, $n = 4$), the experimental band gap was reported to be 5.11 ± 0.02 eV. Rodríguez and coworkers [32] reported a calculated band gap in the vicinities of 5.0 eV for the α-, β-, and γ-phases. In this work, calculated band gaps for the new stable phases of glycine are 5.8 (orthorhombic), 6.8 (tetragonal), and 7.5 (monoclinic) eV, as shown in Fig. 3. Thus, for all crystals listed above, calculated and experimental band gaps place them in the insulator category.

5. Mechanical properties

Attempts to understand the conditions for mechanical stability of crystalline structures date back to the works of Max Born and coauthors in the 1940s [56,57]. A set of necessary and sufficient conditions known

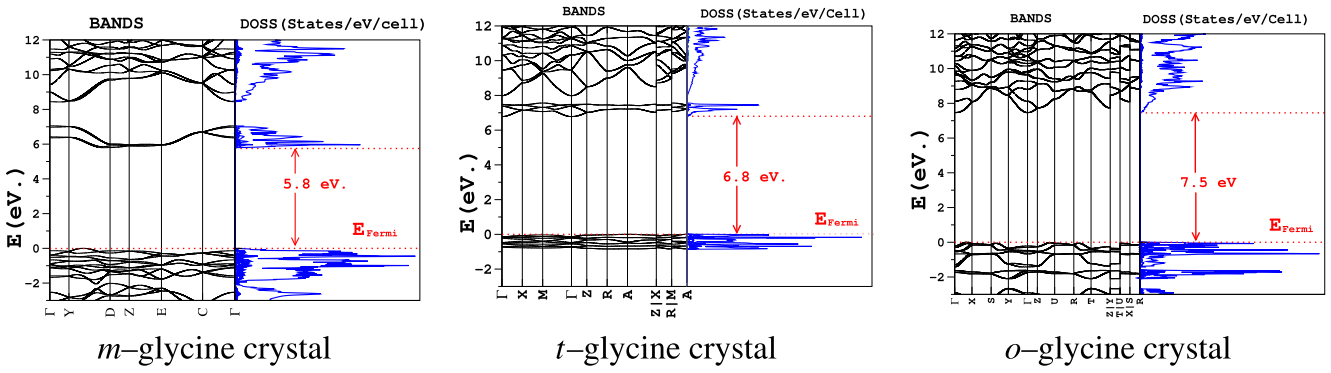

Fig. 3. Bands and DOS for glycine crystal structures.

as *Born stability criteria*, for each crystal symmetry, were developed as a function of elasticity constants. For each spatial group, the elasticity tensor can be reduced to a 6×6 symmetric elasticity matrix [58]. The Born stability criteria for each crystal phase are written in terms of the elasticity matrix elements as [58]

$$c_{ii} > 0, \quad c_{33}c_{55} - c_{35}^2 > 0,$$
$$c_{44}c_{66} - c_{46}^2 > 0, \quad c_{22} + c_{33} - 2c_{23} > 0,$$
$$c_{11} + c_{22} + c_{33} + 2(c_{12} + c_{13} + c_{23}) > 0 \tag{2}$$

$$c_{11} > |c_{12}|, \quad 2c_{13} < c_{33}(c_{11} + c_{12}), \quad c_{44} > 0,$$
$$2c_{16}^2 < c_{66}(c_{11} - c_{12}) \tag{3}$$

$$c_{11} > 0, \ c_{44} > 0, \ c_{55} > 0, \ c_{66} > 0, \quad c_{11}c_{22} > c_{12}^2,$$
$$c_{11}c_{22}c_{33} + 2c_{12}c_{13}c_{23} - c_{11}c_{23}^2 - c_{22}c_{13}^2 - c_{33}c_{12}^2 > 0 \tag{4}$$

for the monoclinic (Eq. (2)), tetragonal (Eq. (3)), and orthorhombic (Eq. (4)) phases, respectively. We provide the corresponding matrices in Tables 4–6.

As can be seen from Tables 4–6, all new phases of glycine crystals satisfy the conditions for mechanical stability. Our results suggest that the response of orthorhombic crystals against linear compression is anisotropic ($c_{11} = 138.63 > c_{22} = 44.13 > c_{33} = 18.44$ GPa). Conversely, the response of tetragonal crystals against linear compression exhibits two dimensional isotropy ($c_{11} = 16.29 = c_{22} = 16.29 < c_{33} = 49.75$ GPa), and the response of monoclinic crystals is quasi isotropic in all directions.

Table 7 lists the values of the Shear (G) and Young (E) moduli, as well as the mechanical hardness (H), and the Poisson (ν) and Pugh (κ) ratios for the three new stable crystalline phases of glycine.

The Bulk (B) and Shear (G) moduli measure the resistance of a material to change in size and shape, respectively. The $\kappa = G/B$ ratio, known as the Pugh criterion [59], is associated to ductility ($\kappa < 0.57$) or to fragility ($\kappa > 0.57$). Accordingly, the orthorhombic phase is predicted to be fragile while the monoclinic and tetragonal phases are characterized as ductile.

The Young modulus (E), defined as the ratio between applied stress and the resulting strain within the elasticity limit, provides information about the rigidity of the crystals. Our computational results show that the Young moduli for the new stable phases of glycine are not too far from the experimentally measured moduli of several amino acid crystals, such as α-glycine, γ-glycine, L-Alanine and DL-Serine, whose measured moduli are in the 20.8 ± 0.4 to 44 ± 1 GPa range [60].

Compressibility is determined using the Poisson ratio, whose maximum value, 0.5, would be achieved only in ideal, perfectly incompressible isotropic materials [61,62]. The values of the Poisson ratio for the new m, t, o polymorphs of glycine place them in the compressibility range of common materials such as metallic glasses for example [63]. The mechanical hardness of a material is related to local plastic deformation. Under this premise, hardness (in GPa) of polymorphs may be estimated by [64]

$$H \approx 2(\kappa^2 G)^{0.585} - 3 \tag{5}$$

Our results for the new stable phases of glycine are not too far from experimental hardness for known glycine crystals, which are reported to be ≈ 0.5 GPa [65,66]. Since mechanical hardness for all polymorphs of glycine (new and known) are smaller that 10 GPa, all of them are characterized as soft materials.

Table 4
Symmetric elasticity matrix for the orthorhombic phase of glycine crystals in GPa.

138.63	33.40	6.79	0	0	0
	44.13	2.19	0	0	0
		18.44	0	0	0
			2.99	0	0
				5.96	0
					33.48

Table 5
Symmetric elasticity matrix for the tetragonal phase of glycine crystals in GPa.

16.29	15.14	13.72	0	0	0.44
	16.29	13.72	0	0	−0.44
		49.75	0	0	0
			14.57	0	0
				14.57	0
					7.28

Table 6
Symmetric elasticity matrix for the monoclinic phase of glycine crystals in GPa.

43.40	20.87	12.00	0	3.35	0
	36.71	14.12	0	2.79	0
		42.32	0	6.49	0
			12.99	0	2.97
				7.88	0
					15.88

Table 7
Descriptors of mechanical stability of the new stable phases of glycine. G: Shear modulus. E: Young modulus. ν: Poisson ratio. κ: Pugh ratio. H: mechanical hardness. All data in GPa.

Crystal	G	E	ν	κ	H
monoclinic	12.38	29.61	0.28	0.52	1.01
tetragonal	9.93	16.35	0.34	0.53	0.67
orthorhombic	19.07	33.37	0.26	0.60	3.18

Table 8
QTAIM derived periodic descriptors of the nature of intermolecular bonding interactions (hydrogen bonds, HB, and the N···COO interaction in *o*-glycine) in *m*-, *o*- and *t*-glycine crystals. All data taken from optimized geometries at the B3LYP level in conjunction with a triple-zeta valence plus polarization basis set level of theory. d_{HB} in Å: distances between the two participating moeities. E_{HB} in kJ/mol: approximate energies of the hydrogen bonds, estimated using the Espinosa-Molins-Lecomte formula: $E_{HB} = 0.5V(\mathbf{r}_c)$ [76]. All other parameters in a.u. See Fig. 2 for atom labels.

Crystal	Atoms	d_{HB}	$10^2 \times \rho(\mathbf{r}_c)$	$10^2 \times \nabla^2\rho(\mathbf{r}_c)$	$\lvert\mathscr{V}(\mathbf{r}_c)\rvert/\mathscr{G}(\mathbf{r}_c)$	$\mathscr{H}(\mathbf{r}_c)/\rho(\mathbf{r}_c)$	E_{HB}
m	NH8···O2	1.85	3.3	10.3	1.02	−0.02	−35.36
	NH6···O2	1.88	2.9	10.0	0.95	0.04	−30.06
	NH7···O2	1.98	2.3	8.6	0.88	0.10	−22.13
	CH10···O1	2.18	1.6	6.0	0.81	0.14	−13.52
	CH9···O1	2.43	1.2	4.3	0.79	0.16	−9.14
t	NH8···O2	1.73	4.2	12.5	1.11	−0.09	−50.96
	NH6···O2	1.81	3.5	11.6	1.03	−0.02	−40.35
	NH7···O1	1.86	2.9	10.5	0.94	0.05	−30.71
	CH9···O1	2.13	1.8	6.8	0.82	0.15	−15.33
o	N···COO	1.57	21.1	−37.0	3.20	−0.80	not a HB
	NH6···O2	1.62	6.0	14.0	1.28	−0.23	−82.11
	OH···O2	1.72	4.1	12.8	1.10	−0.08	−50.71
	NH8···O1	2.17	2.1	8.9	0.91	0.09	−24.47
	CH10···O2	2.56	0.7	2.5	0.72	0.19	−4.65
	CH9···O1	2.67	0.7	2.4	0.75	0.17	−4.71

5.1. Intermolecular bonding interactions

Properties of bond critical points ($\mathbf{r}_c$,BCPs) for all intermolecular interactions leading to stability in the new phases of glycine crystals calculated using the formalism of the quantum theory of atoms in molecules (QTAIM) [67] as implemented for periodic systems in CRYSTAL-14 [24,25] are listed in Table 8 and plotted in Fig. 4. Several useful descriptors discussed elsewhere [67] were used to dissect the nature of bonding interactions. We summarize our findings as follows:

1. Considering that all intermolecular interactions are hydrogen bonds (except for the N···COO contacts in *o*-glycine), the calculated

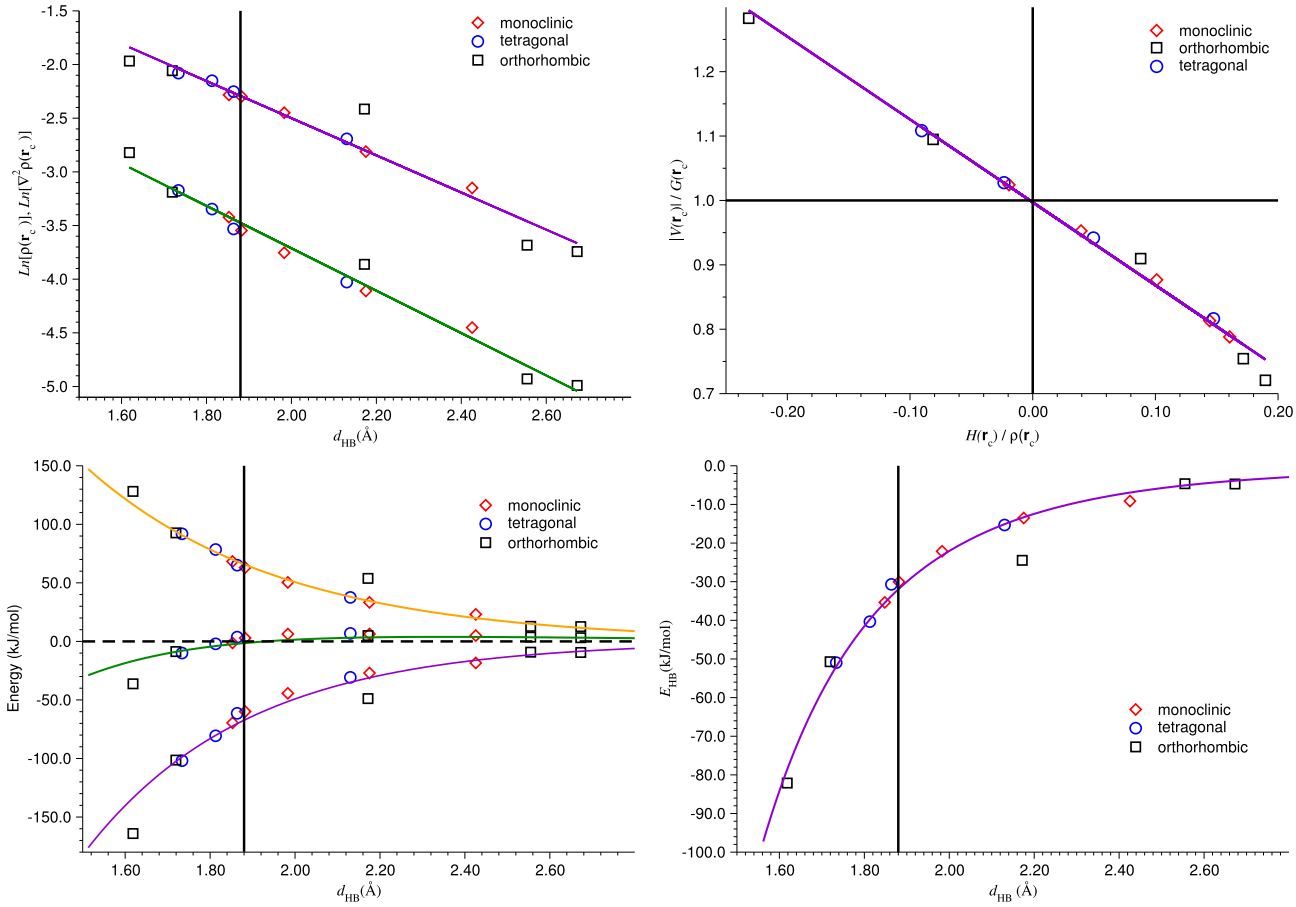

Fig. 4. Descriptors of the nature of bonding intermolecular interactions derived from the periodic topological properties of the electron densities at bond critical points. Top left: exponential decays of electron densities ($\rho(\mathbf{r}_c)$, green line) and of their Laplacians ($\nabla^2\rho(\mathbf{r}_c)$, purple line). Top right: Espinosa's criterion [76]. Bottom left: kinetic (orange line), potential (purple line), and total (green line) energy densities as a function of the length of hydrogen bonds. Bottom right: Approximate energy of the hydrogen bonds as a function of length. Vertical lines at 1.88 Å mark the boundary between closed shell and intermediate interactions (see text).

separations between the two participating units cover a wide range, from the unusually short and strong NH6···O2 to the very long and weak secondary CH9···O1 HB.

2. The values of electron densities at BCPs for hydrogen bonds in the new stable phases of glycine crystals fall in the range of several related hydrogen bonds [68–75]. Accumulation of electron density, $\rho(\mathbf{r}_c)$, around a given BCP, for an intermolecular interaction indicates the extent to which the two participating moeities share their electrons, and thus is an approximate measure of covalency. It is clear from Table 8 for all hydrogen bonds that these are weak interactions because the electron density at BCPs is about one entire order of magnitude smaller than for example the strong N···COO contact. The top left panel of Fig. 4 shows an exponential decay of the electron density around BCPs associated to hydrogen bonds as a function of the length of the hydrogen bond. There are two important aspects worth mentioning: on one hand, the exponential decay correctly describes the asymptotic behavior, which at large distances leads to no BPC and to no shared electron density; on the other hand, all types of hydrogen bonds for all phases obey the same correlation, thus, they are clearly interactions of the same physical nature.
3. The Laplacian of a function is a mathematical tool for the characterization of local extrema as either local maxima or minima. Thus, for the particular case of the electron density, it is a measure of local concentration or depletion of electron charge [77]. Indeed, local minima (positive Laplacians) at BCPs describe interactions where the electron density is displaced away from the critical point, towards the nuclei, a characteristic of long range and of ionic interactions. Conversely, local maxima (negative Laplacians) at BCPs describe interactions where the electron density is concentrated in the internuclear region, around the BCP, a characteristic of covalent bonding. In this context, the results listed in Table 8 reveal only ionic and/or long range interactions in the hydrogen bonds (all have positive Laplacians) leading to crystal stabilization. Nicely, the very strong C···COO interaction in *o*-glycine is described by the Laplacian of the electron density as highly covalent. An exponential decay as a function of distance with the same benefits as explained above for the electron densities is seen on the left top left panel of Fig. 4.
4. Energy densities have units of pressure. Therefore, local energy densities may be equated to the local quantum pressure on the electron cloud [77]. Accordingly, local positive energy densities may be physically interpreted as regions from where the electrons want to escape, leading to local depletion of charge. Similarly, negative energy densities may be physically interpreted as regions that suck in neighboring electrons, leading to local concentration of charge. The everywhere positive (repulsive) kinetic energy, and the everywhere negative (attractive) potential energy fit this interpretation perfectly as can be seen in the bottom left panel of Fig. 4. As a consequence, the sign of the resulting local total energy density $\mathscr{H}(\mathbf{r}_c) = \mathscr{G}(\mathbf{r}_c) + \mathscr{V}(\mathbf{r}_c)$, a measure of the balance between the repulsive and attractive interactions, is a good criterion for the nature of the stabilizing interactions. Fig. 4 shows a few points with negative total energy densities, with hydrogen bond lengths smaller than 1.88 Å, the distance at which the repulsive interactions begin to slightly dominate (the same observation may be drawn from Table 8). This is an early indication that notwithstanding the fact that all hydrogen bonds in the new stable phases of glycine have the same physical origins (see the above discussion on electron densities at BCPs), they are not equivalent in their nature.
5. Local application of the virial theorem at BCPs lead Espinosa and coworkers [76] to establish a more detailed and somewhat quantitative description of bonding interactions. In this picture, critical points with larger contributions from the repulsive kinetic energy described by $|\mathscr{V}(\mathbf{r}_c)|/\mathscr{G}(\mathbf{r}_c) < 1$, characterize long range or ionic interactions, critical points with excess of locally stabilizing potential energy, that is, those for which $|\mathscr{V}(\mathbf{r}_c)|/\mathscr{G}(\mathbf{r}_c) > 2$, characterize covalent bonds, and the intermediate region $1 < |\mathscr{V}(\mathbf{r}_c)|/\mathscr{G}(\mathbf{r}_c) < 2$, contains all types of bonding interactions with contributions from both, long range and covalent types. The top right panel of Fig. 4 and the data listed in Table 8 uncover a picture fully consistent with the above discussion of energy densities: not all hydrogen bonds stabilizing the new phases of glycine are equivalent, most of them are of long range type, mostly van der Waals or London as well as ionic, but a few very strong ones are of the intermediate character. It is worth noticing that this intermediate character bonding interactions may be traced back to the early formal application of quantum mechanics to chemical bonding by Pauling [78] and by Coulson [79] in which wave functions were written as linear combinations of all possibilities. In related studies of hydrogen bonds [80], it has been shown that covalency and ionicity are not incompatible features of HBs, rather, they seem to act concomitantly.
6. Approximate energies for hydrogen bonds may be estimated using the Espinosa-Molins-Lecomte formula [76] $E_{HB} = 0.5V(\mathbf{r}_c)$. The results listed in Table 8 and plotted in Fig. 4 are quite revealing: including all types of HBs and all new stable phases of glycine, the collective data perfectly fits the attractive $1/r^6$ region of a Lennard-Jones potential [81].
7. The collective topological descriptors of chemical bonding gathered at bond critical points suggest that the NH6···O2 hydrogen bond in the new *o*-phase of glycine crystals is unusually strong, having negative energy density, the largest accumulation of electron density, the smallest interaction distance, and the largest virial ratio.

6. Summary and conclusions

Explorations of the potential energy surfaces for glycine crystals afford three new orthorhombic, tetragonal, and monoclinic stable phases, with properties close to the experimentally known α, β, and γ-glycine. The new crystals passed all tests designed to establish thermodynamic (large negative cohesion energies provided by networks of typical NH···O and OH···O and secondary CH···O hydrogen bonds), dynamic (phonon vibrations), and mechanical (Born conditions) stability. Tetragonal and monoclinic crystals are ductile while orthorhombic crystals are characterized as fragile. All phases have low mechanical hardness, classifying them as soft materials, all are compressible, in the same order of common metallic glasses. Band gaps for the new crystalline phases of glycine cover the 5.8–7.5 eV range, characterizing them as insulators. Not all hydrogen bonds are equivalent, a number of them are predicted to be long range contacts with some degree of covalency. Put together, all types of HBs and all new stable phases of glycine, the collective data perfectly fits the attractive $1/r^6$ region of a Lennard-Jones potential.

Declaration of Competing Interest

The authors declare that they have no known competing financial interests or personal relationships that could have appeared to influence the work reported in this paper.

Acknowledgements

Partial financial support for this project was provided by Universidad de Antioquia via “Estrategia para la sostenibilidad”. Funding by internal EAFIT projects is also Acknowledged.

References

[1] M. Stroncio, M. Dutta, Integrated biological-semiconductor device, Proc. IEEE 93 (2005) 1772–1783.
[2] P.R. Tulip, S. Clark, Structural and electronic properties of L-amino acids, Phys. Rev. B 71 (2005) 195117 .
[3] M.Z.S. Flores, V.N. Freire, R.P. dos Santos, G.A. Farias, E.W.S. Caetano, M.C.F. de Oliveira, J.R.L. Fernandez, L.M.R. Scolfaro, M.J.B. Bezerra, T.M. Oliveira,

G.A. Bezerra, B.S. Cavada, H.W. Leite Alves, Optical absorption and electronic band structure first-principles calculations of α– glycine crystals, Phys. Rev. B 77 (2008) 115104 .
[4] J.A. Chisholm, S. Motherwell, P.R. Tulip, S. Parsons, S.J. Clark, An ab initio study of observed and hypothetical polymorphs of glycine, Cryst. Growth Des. 5 (2005) 1437–1442.
[5] T.P. Srinivasan, R. Indirajith, R. Gopalakrishnan, Growth and characterization of α and γ-glycine single crystals, J. Cryst. Growth Des. 318 (2011) 762–767.
[6] E. Seyedhosseini, K. Romanyuk, D. Vasileva, S. Vasilev, A. Nuraeva, P. Zelenovskiy, M. Ivanov, A.N. Morozovska, V.Ya. Shur, H. Lu, A. Gruverman, A.L. Kholkin, Self-assembly of organic ferroelectrics by evaporative dewetting: a case of β–glycine, ACS Appl. Mater. Interfaces 9 (2017) 20029–20037.
[7] A. Heredia, V. Meunier, I.K. Bdikin, J. Gracio, N. Balke, S. Jesse, A. Tselev, P. Agarwal, B.G. Sumpter, S.V. Kalinin, A.L. Kholkin, Nanoscale ferroelectricity in crystalline γ-glycine, Adv. Funct. Mater. 22 (2012) 2996–3003.
[8] P. Hu, S. Hu, Y. Huang, J. Reimers, A. Rappe, Y. Li, A. Stroppa, W. Wei Ren, Bioferroelectric properties of glycine crystals, J. Phys. Chem. Lett. 10 (2019) 1319–1324.
[9] L. Yu, J. Huang, K. Jones, Measuring free-energy difference between crystal polymorphs through eutectic melting, J. Phys. Chem. B 109 (2005) 19915–19922.
[10] G.L. Perlovich, L.K. Hansen, A. Bauer-Brandl, The Polymorphism of Glycine Thermochemical and structural aspects, J. Therm. Anal. Cal. 166 (2001) 699–715.
[11] K. Srinivasan, Crystal growth of α and γ glycine polymorphs and their polymorphic phase transformations, J. Crystal Growth 311 (2008) 156–162.
[12] S. Goryainov, E. Boldyreva, E. Kolesnik, Raman observation of a new (ξ) polymorph of glycine, Chem. Phys. Lett. 419 (2006) 496–500.
[13] N. Marom, R.A. DiStasio Jr., V. Atalla, S. Levchenko, A.M. Reilly, J.R. Chelikowsky, L. Leiserowitz, A. Tkatchenko, Many-body dispersion interactions in molecular crystal polymorphism, Angew. Chem. Int. Ed. 52 (2013) 6629–6632.
[14] P. Bulutoglu, C. Parks, N. Nere, S. Bordawekar, D. Ramkrishna, Processes 7 (2019) 268.
[15] A. Mei, X. Luo, RSC Adv. 9 (2019) 3877.
[16] A. Heredia, M. Colín-García, T. Puig, L. Alba-Aldave, A. Meléndez, J. Cruz-Castañeda, V. Basiuk, S. Ramos-Bernal, A. Negrón, BioSystems 162 (2017) 66.
[17] A.R. Oganov, C.W. Glass, Crystal structure prediction using ab initio evolutionary techniques: Principles and applications, J. Chem. Phys. 124 (2006) 244704–244715.
[18] C.W. Glass, A.R. Oganov, N. Hansen, USPEX – evolutionary crystal structure prediction, Comput. Phys. Commun. 175 (2006) 713–720.
[19] A.R. Oganov, A.O. Lyakhov, M. Valle, How evolutionary crystal structure prediction works – and why, Acc. Chem. Res. 44 (2011) 227–237.
[20] B. Narayana Moolya, A. Jayarama, M. Sureshkumar, S. Dharmaprakash, J. Cryst. Growth 205, 280, 581.
[21] P. Hohenberg, W. Kohn, Inhomogeneous electron gas, Phys. Rev. 136 (1964) B864–B871.
[22] W. Kohn, L.J. Sham, Self-consistent equations including exchange and correlation effects, Phys. Rev. 140 (1965) A1133–A1138.
[23] R.O. Jones, O. Gunnarsson, The density functional formalism, its applications and prospects, Rev. Mod. Phys. 61 (1989) 689–746.
[24] R. Dovesi, R. Orlando, B. Civalleri, R. Roetti, V.R. Saunders, C.M. Zicovich-Wilson, CRYSTAL: a computational tool for the ab initio study of the electronic properties of crystals, Z. Kristallogr. 220 (2005) 571–573.
[25] R. Dovesi, V.R. Saunders, R. Roetti, R. Orlando, C.M. Zicovich-Wilson, F. Pascale, B. Civalleri, K. Doll, N.M. Harrison, I.J. Bush, P. D'Arco, M. Llunell, CRYSTAL09 User's Manual, University of Torino Torino, 2009 URL:http://www.crystal.unito.it.
[26] A.D. Becke, Density–functional thermochemistry. III. The role of exact exchange, J. Chem. Phys. 98 (1993) 5648–5652.
[27] S.H. Vosko, L. Wilk, M. Nusair, Accurate spin–dependent electron liquid correlation energies for local spin density calculations: a critical analysis, Can. J. Phys. 58 (1980) 1200–1211.
[28] C. Lee, W. Yang, R.G. Parr, Development of the Colic-Salvetti correlation–energy formula into a functional of the electron density, Phys. Rev. B 37 (1988) 785–789.
[29] M.F. Peintinger, D.V. Oliveira, T. Bredow, Consistent gaussian basis sets of triple-zeta valence with polarization quality for solid-state calculations, J. Comput. Chem. 34 (2013) 451–459.
[30] H.J. Monkhorst, J.D. Pack, Special points for Brillonin–zone integrations, Phys. Rev. B 13 (1976) 5188–5192.
[31] A. Dawson, D.R. Allan, S.A. Belmonte, S.J. Clark, W.I.F. David, P.A. McGregor, S. Parsons, C.R. Pulham, L. Sawyer, Effect of high pressure on the crystal structures of polymorphs of glycine, Cryst. Growth Des. 5 (2005) 1415–1427.
[32] J. Rodríguez, G. Costa, M. da Silva, B. Silva, L. Honório, P. de Lima-Neto, R. Santos, E. Caetano, H. Alves, V. Freire, Crys. Growth. Des. 19 (2019) 5204.
[33] B. Civaller, C.M. Zicovich-Wilson, L. Valenzano, P. Ugliengo, B3LYP augmented with an empirical dispersion term (B3LYP-D*) as applied to molecular crystals, Cryst. Eng. Commun. 10 (2008) 405–410.
[34] S. Grimme, Semiempirical GGA–type density functional constructed with a long-range dispersion correction, J. Comput. Chem. 27 (2006) 1787–1799.
[35] F. Pascale, C.M. Zicovich-Wilson, F. Lopez Gejo, B. Civaller, R. Orlando, R. Dovesi, The calculation of the vibrational frequencies of crystalline compounds and its implementation in the CRYSTAL code, J. Comput. Chem. 25 (2004) 888–897.
[36] Q. Jiang, A.G. Shtukenberg, M.D. Ward, Ch. Hu, Non-topotactic phase transformations in single crystals of β-glycine, Cryst. Growth Des. 15 (2015) 2568–2573.
[37] Y. Iitaka, The crystal structure of β-glycine, Acta Crystallogr. 13 (1960) 35–45.
[38] T.N. Drebushchak, E.V. Boldyreva, E.S. Shutova, β-Glycine, Acta Crystallogr. Sect. E 58 (2002) o634–o636.
[39] Y. Iitaka, The crystal structure of γ-glycine, Acta Crystallogr. 14 (1961) 1–10.
[40] J.-P. Legros, Å. Kvick, Deformation electron density of α-Glycine at 120K, Acta Cryst. B36 (1980) 3052–3059.
[41] Å. Kvick, An experimental study of the influence of temperature on a hydrogen-bonded system: the crystal structure of γ-glycine at 83 K and 298 K by neutron diffraction, Acta Crystallogr. B 36 (1980) 115–120.
[42] E.V. Boldyreva, V.A. Drebushchak, T.N. Drebushchak, I.E. Paukov, Y.A. Kovalevskaya, E.S. Shutova, Polymorphism of Glycine Thermodynamic aspects. Part I. Relative stability of the polymorphs, J. Therm. Anal. Cal. 73 (2003) 409–418.
[43] C.E. Hughes, K.D.M. Harris, Direct observation of a transient polymorph during crystallization, Chem. Commun. 46 (2010) 4982–4984.
[44] V.A. Drebushchaka, E.V. Boldyreva, T.N. Drebushchakb, E.S. Shutova, Synthesis and calorimetric investigation of unstable β–glycine, J. Cryst. Growth 241 (2002) 266–268.
[45] D. Isakov, D. Petukhova, S. Vasilev, A. Nuraeva, T. Khazamov, E. Seyedhosseini, P. Zelenovskiy, V. Ya Shur, A.L. Kholkin, In Situ observation of the humidity controlled polymorphic phase transformation in glycine microcrystals, Cryst. Growth Des. 8 (2014) 4138–4142.
[46] M. Born, K. Huang, Dynamical Theory of Crystal Lattices, Clarendn, Oxford, 1954.
[47] R. Mittal, S.L. Chaplot, N. Choudhury, Modeling of anomalous thermodynamic properties using lattice dynamics and inelastic neutron scattering, Prog. Mater. Sci. 51 (2006) 211–286.
[48] A. van de Walle, M. Asta, G. Ceder, The alloy theoretic automated toolkit: a user guide, Calphad 26 (2002) 539–553.
[49] Y. Wang, Z.-K. Liu, L.Q. Chen, Thermodynamic properties of Al, Ni, NiAl, and Ni_3 Al from first-principles calculations, Acta Mater. 52 (2004) 2665–2671.
[50] Y. Wang, J.J. Wang, H. Zhang, V.R. Manga, S.L. Shang, L.-Q. Chen, Z-K. Liu, A first-principles approach to finite temperature elastic constants, J. Phys. Condens. Matter 22 (2010) 225404–225408.
[51] A. Chernatynskiy, S.R. Phillpot, Phonon transport simulator (PhonTS), Comput. Phys. Commun. 192 (2015) 196–204.
[52] W. Li, J. Carrete, N.A. Katcho, N. Mingo, ShengBTE: a solver of the Boltzmann transport equation for phonons, Comput. Phys. Commun. 185 (2014) 1747–1758.
[53] A. Togo, L. Chaput, I. Tanaka, Distributions of phonon lifetimes in Brillouin zones, Phys. Rev. B 91 (2015) 094306 .
[54] S.N. Costa, F.A.M. Sales, V.N. Freire, F.F. Maia Jr., E.W.S. Caetano, L.O. Ladeira, E.L. Albuquerque, U.L. Fulco, L-serine anhydrous crystals: structural, electronic, and optical properties by first-principles calculations, and optical absorption measurement, Cryst. Growth Des. 13 (2013) 2793–27803.
[55] J.R. Cândido-Júnior, F.A.M. Sales, S.N. Costa, P. De Lima-Neto, D.L. Azevedo, E.W.S. Caetano, E.L. Albuquerque, V.N. Freire, Monoclinic and orthorhombic cysteine crystals are small gap insulators, Chem. Phys. Lett. 512 (2011) 208–210.
[56] M. Born, On the stability of crystal lattices, I. Math. Proc. Camb. Phil. Soc. 36 (1940) 160–172.
[57] M. Born, K. Huang, Dynamics Theory of Crystal Lattices, Oxford University Press, 1954.
[58] F. Mouhat, F.-X. Coudert, Necessary and sufficient elastic stability conditions in various crystal systems, Phys. Rev. B 90 (2014) 224104 .
[59] S.F. Pugh, XCII. Relations between the elastic moduli and the plastic properties of polycrystalline pure metals Philos, Philos. Mag. 45 (1954) 823–843.
[60] I. Azuri, E. Meirzadeh, D. Ehre, S.R. Cohen, A.M. Rappe, M. Lahav, I. Lubomirsky, L. Kronik, Unusually large young's moduli of amino acid molecular crystals, Angew. Chem. Int. Ed. 54 (2015) 13566–13570.
[61] P.H. Mott, J.R. Dorgan, C.M. Roland, The bulk modulus and Poisson's ratio of incompressible materials, J. Sound Vib. 312 (2008) 572–575.
[62] P.H. Mott, C.M. Roland, Limits to Poisson's ratio in isotropic materials, Phys. Rev. B 80 (2009) 132104 .
[63] W.H. Wang, Correlation between relaxations and plastic deformation, and elastic model of flow in metallic glasses and glass-forming liquids, J. Appl. Phys. 110 (2011) 053521 .
[64] X.-Q. Chen, H. Niu, D. Li, Y. Li, Modeling hardness of polycrystalline materials and bulk metallic glasses, Intermetallics 19 (2011) 1275–1281.
[65] S.A. Azhagan, S. Ganesan, Structural, mechanical, optical and second harmonic generation (SHG) studies of gamma glycine single crystal, Int. J. Phys. Sci. 8 (2013) 6–11.
[66] K. Ambujam, S. Selvakumar, D.P. Anand, G. Mohamed, P. Sagayaraj, Cryst. Res. Technol. 41 (2006) 671–677.
[67] R.F.W. Bader, Atoms in Molecules: A Quantum Theory, Clarendon Press, Oxford, 1990.
[68] A.D. Zapata-Escobar, J.A. Murillo-López, C.Z. Hadad, A. Restrepo, Understanding the nature of bonding interactions in the carbonic acid dimers, J. Mol. Model. 25 (2019) 20.
[69] P. Farfán, A. Echeverri, E. Diaz, J.D. Tapia, S. Gómez, A. Restrepo, Dimers of formic acid: structures, stability, and double proton transfer, J. Chem. Phys. 147 (2017) 044312 .
[70] C. Ibargüen, D. Guerra, C.Z. Hadad, A. Restrepo, Very weak interactions: structures, energies and bonding in the tetramers and pentamers of hydrogen sulfide, RSC Adv. 4 (2014) 58217–58225.
[71] F. Ramírez, C.Z. Hadad, D. Guerra, J. David, A. Restrepo, Structural studies of the water pentamer, Chem. Phys. Lett. 507 (2011) 229–233.
[72] C.Z. Hadad, A. Restrepo, S. Jenkins, F. Ramírez, J. David, Hydrophobic meddling in small water clusters, Theor. Chem. Acc. 132 (2013) 1376.
[73] C.Z. Hadad, E. Florez, N. Acelas, G. Merino, A. Restrepo, Microsolvation of small cations and anions, Int. J. Quantum Chem. 119 (2019) e25766 .
[74] E. Florez, N. Acelas, C. Ibargüen, S. Mondal, J.L. Cabellos, G. Merino, A. Restrepo, Microsolvation of NO_3^-: structural exploration and bonding analysis, IRSC Adv. 6

(2016) 71913–71923.
[75] D. Guerra, J. David, A. Restrepo, (H3N–BH3)4: the ammonia borane tetramer, Phys. Chem. Chem. Phys. 14 (2012) 14892–14897.
[76] E. Espinosa, E. Molins, C. Lecomte, Hydrogen bond strengths revealed by topological analyses of experimentally observed electron densities, Chem. Phys. Lett. 285 (1998) 170–173.
[77] P.L. Popelier, Atoms in Molecules: An Introduction, Prentice Hall, Harlow, 2000.
[78] P. Linus, The Nature of the Chemical Bond and the Structure of Molecules and Crystals: An Introduction to Modern Structural Chemistry, Cornell University Press, Ithaca, New York, 1939.
[79] C.A. Coulson, Valence, Oxford University Press, 1961.
[80] E. Florez, N. Acelas, F. Ramírez, C.Z. Hadad, A. Restrepo, Microsolvation of F^-, Phys. Chem. Chem. Phys. 20 (2018) 8909–8920.
[81] J.E. Lennard-Jones, Cohesion, Proc. Phys. Soc. 43 (1931) 461–482.